SPARC: UNIFIED FRAMEWORK FOR AUTOMATIC SEGMENTATION, PROBABILISTIC ATLAS CONSTRUCTION, REGISTRATION AND CLUSTERING OF BRAIN MR IMAGES

Annemie Ribbens, Jeroen Hermans, Frederik Maes, Dirk Vandermeulen, Paul Suetens

Center for Processing Speech and Images - PSI, Department of Electrical Engineering - ESAT
Faculty of Engineering
Katholieke Universiteit Leuven

ABSTRACT

Automated methods for image segmentation, image registration, clustering of images and probabilistic atlas construction are of great interest in medical image analysis. In this work, we propose a model where these different aspects are combined in one comprehensive probabilistic framework. The framework is formulated as an EM optimization algorithm. Validation is performed on simulated and real images in terms of segmentation, clustering and atlas construction. Accurate segmentations are obtained and the different modes in a population of normal controls and Huntington disease patients are discovered. Furthermore, our method reveals the localization of cluster specific morphological differences for each image in the population.

Index Terms— Segmentation, Clustering, Probabilistic Atlas Construction, Registration

1. INTRODUCTION

Segmentation of relevant brain structures in MR images can provide important information about neurological diseases and their progression. However, manual delineation of these structures is time consuming and susceptible to inter- and intra-observer variability. Therefore, there is a need for automated brain image segmentation methods. Such methods often rely on probabilistic brain atlases, i.e. templates representing the average brain anatomy of populations and their variability which can be constructed in many different ways [1, 2, 3, 4]. Their performance can be improved by using brain atlases better adapted towards the images to be segmented. This can be achieved for instance by creating and selecting appropriate population-, subgroup- or even subject-specific atlases [5, 6]. In [5], images of a population are clustered into different subgroups which are used to create subgroup-specific atlases. In [6], atlases are directly constructed in the space of the image to be segmented. It must be noted that also the brain atlases and clustering methods themselves are of great interest in medical image analysis as they allow the investigation of structural and functional characteristics. The atlases show a mean template and the variability in a population, while the clustering helps us to find new subgroups, to understand and discover structural differences and similarities between the subgroups and to localize these differences.

Another way to create atlases well adapted to the image to be segmented is by using atlas-to-image registration techniques [7]. Moreover, recently, probabilistic models have been presented which combine atlas-based registration with an intensity-based segmentation model in one unified framework [8, 9, 10]. As such both techniques cooperate to obtain the final segmentation result. Finally, some techniques avoid the use of an atlas by segmenting a group of images simultaneously and hence build models (priors) implicitly or explicitly during the algorithm [11, 12, 13].

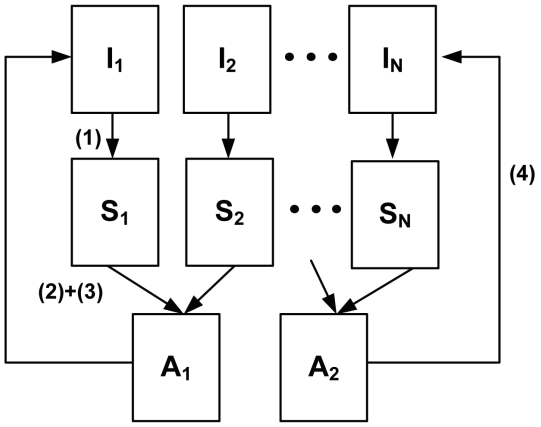

Fig. 1. Total scheme of framework: (1) Segmentation using previous estimation of atlases and Gaussian mixture model, (2) Clustering, (3) Atlas formation, (4) Atlas-to-image registration.

In this paper, we present a comprehensive probabilistic model that captures the previously described techniques from literature in one unified framework where they can all benefit from each other. This framework, called **SPARC**, is presented in Figure 1 and iteratively estimates the **S**egmentation of the images, the **P**robabilistic **A**tlases per cluster, the atlas-to-image **R**egistrations and the **C**lustering. The model is formulated as a maximum a posteriori (MAP) problem and optimized using an expectation maximization (EM) procedure.

2. METHOD

In this section, we describe a probabilistic model that tries to segment simultaneously a set of brain MR images and clusters them into different subgroups. Our model is defined in such a way that also a probabilistic brain atlas will be constructed for each cluster. Let us denote the image intensities as $Y = \{Y_{ij}\}$ with $i = \{1 \ldots, N_I\}$ the number of images and $j = \{1 \ldots, N_J\}$ the number of vox-

els. Furthermore, let $t = \{1 \ldots, N_T\}$ be the number of clusters and $k = \{1 \ldots, N_K\}$ the number of tissue classes with N_T and N_K fixed by the user. We specify now our model and make some independency assumptions. After correction of the bias field, our model assumes that the image intensities are generated from a Gaussian mixture model with parameters $\theta = \{\mu, \sigma^2\}$ for each tissue class separately. The bias field is estimated as in [14] and we denote the bias field parameters for each image i as C_i. The probability density function on the image intensities can therefore be written as $P(y_{ij}|\theta_{ik}, C_i)$. Furthermore, priors are added to our model. The prior probability of the tissue labeling $L = \{l_{ijk}\}$ is the probability of having tissue class k in voxel j of the atlas t deformed to image i. The probabilistic atlas for cluster t is itself a parameter that needs to be estimated. The prior probability on the labeling can thus be denoted as $P(l_{ijk}|A_{tk}, R_{tij}) = A_{tk}(R_{ti}(j))$ with A_{tk} the probability map of tissue class k in the atlas of cluster t and R_{ti} the atlas-to-image deformation field. Furthermore, a uniform prior is put on the clustering, i.e. parameter π. Lastly, for the prior on the atlas-to-image registration R, we assume that the registration can be modeled as the realization of a random process with a Gaussian probability density function with mean G and variance ϵ^2. Remark that parameter G can be interpreted as a groupwise registration for each cluster between the atlas and the set of images belonging to that cluster. In other words, applying this registration on the estimated atlas, brings the atlas to the space where the least deformation is necessary. The parameter ϵ^2 represents then the variability between the atlas-to-image registration and the groupwise registration. The prior is denoted as $P(R_{tij}|G_{tj}, \epsilon_t)$.
Our model with parameters $\Upsilon = \{\theta, C, A, \pi, R, G, \epsilon^2\}$, needs to be optimized by the following MAP problem:

$$\hat{\Upsilon} = \arg\max_{\Upsilon} \log P(\Upsilon|Y) \propto \arg\max_{\Upsilon} \log P(Y, \Upsilon).$$

An estimation of the segmentation and clustering is straightforward once the model parameters Υ are known. Estimation of the model parameters, in turn, is helped by knowledge of the segmentation and clustering. Therefore, the MAP problem can be rewritten as

$$\hat{\Upsilon} = \arg\max_{\Upsilon} \log \left[\sum_{L,Z} P(Y, L, Z, \Upsilon) \right] \tag{1}$$

with $L = \{l_{ijk}\}$ the tissue labelmaps and $Z = \{z_{it}\}$ the clustering parameters. To solve this problem with hidden variables, we derive a lower bound using Jensen's inequality which we can optimize using the EM algorithm. The Q-function (E-step) can now be written as follows:

$$\begin{aligned} Q(\Upsilon|\Upsilon^\eta) &= E_{L,Z|Y,\Upsilon^\eta} \left[\log P(Y, L, Z, \Upsilon)\right] \\ &\propto \sum_{i=1}^{N_I} \sum_{j=1}^{N_J} \sum_{k=1}^{N_K} \sum_{t=1}^{N_T} P(l_{ijk}, z_{it}|y_{ij}, \Upsilon^\eta_{ijkt}) \cdot [\log P(y_{ij}|\theta_{ik}, C_i) \\ &+ \log P(l_{ijk}|A_{tk}, R_{tij}) + \log P(z_{it}|\pi_{it}) \\ &+ \log P(R_{tij}|G_{tj}, \epsilon_t)] \end{aligned} \tag{2}$$

where η denotes the previous iteration step and where an expression for the posterior can be found using Bayes'rule:

$$\begin{aligned} b_{itjk} &= P(l_{ijk}, z_{it}|y_{ij}, \Upsilon_{ijkt}) \\ &= \frac{P(y_{ij}|\theta_{ik}, C_i) A_{tk}(R_{ti}(j)) \pi_{it} P(R_{tij}|G_{tj}, \epsilon_t)}{\sum_t \sum_k P(y_{ij}|\theta_{ik}, C_i) A_{tk}(R_{ti}(j)) \pi_{it} P(R_{tij}|G_{tj}, \epsilon_t)} \end{aligned}$$

The sum over all clusters t of the posterior gives us the soft segmentations, denoted as p_{ijk}. They can be interpreted as the weighted sum of the 'sub'-classifications p_{ijkt}, obtained using the Gaussian intensity model and the deformed atlas of cluster t. The sum over all tissue classes k of the posterior gives us the probability that a certain voxel j of a certain image i belongs to a certain cluster t (clustering per voxel, denoted as ρ_{itj}). We could average this term over all voxels j to obtain a global clustering parameter. The computation of the clustering itself is interesting as it is a natural mixture of different aspects: the prior on the clustering, the distance between the atlas-to-image registration and the groupwise registration, and the sum over all tissue classes of the subsegmentation p_{ijkt}. This last aspect can be interpreted as looking for an atlas that agrees with the intensity model and is as sharp as possible. For interpretation purposes later on, we remark that $b_{itjk} = \rho_{itj} \cdot p_{ijkt}$.

In the M-step, the parameters are updated by maximization of Q. As the probability density function on the intensities is independent of the number of clusters t and $\sum_t b_{itjk} = p_{ijk}$, the Gaussian mixture parameters and the bias field parameters are completely similar as in [14].
The atlases, the atlas-to-image registrations and the groupwise registrations have to be updated simultaneously because they depend on each other. Instead, we start with updating the groupwise registration and the atlases making use of the atlas-to-image registration of previous iteration. For the groupwise registration G we find:

$$\frac{\partial Q}{\partial G_{tj}} = 0 \Rightarrow G_{tj} = \frac{\sum_i \rho_{itj} R_{tij}}{\sum_i \rho_{itj}}. \tag{3}$$

The atlases, given the atlas-to-image registrations, can be determined as follows:

$$\frac{\partial Q}{\partial A_{kt}} = \sum_i \frac{\rho_{it}(R_{it}^{-1}(u)) p_{ikt}(R_{it}^{-1}(u))}{A_{kt}(u)} |Jac(R_{it}^{-1}(u))| = 0$$

where we interpret our discrete lattice temporarily as continuum. In other words, the equation is obtained by rewriting the sum over the voxels j as an integral and using the substitution $u = R_{it}(j)$. This equation together with the constraint that $\sum_k A_{kt}(u) = 1$ for all t and all u, gives us the following solution for the atlas:

$$A_{kt}^{\text{new}}(u) = \frac{\sum_i \rho_{it}(R_{it}^{-1}(u)) p_{ikt}(R_{it}^{-1}(u)) |Jac(R_{it}^{-1}(u))|}{\sum_i \rho_{it}(R_{it}^{-1}(u)) |Jac(R_{it}^{-1}(u))|} \tag{4}$$

However, we are looking for voxel $j = R_{it}^{-1}(u)$ in the space of image i. Therefore, the atlas needs to be registered towards the image space using previous atlas-to-image registration R_{it}: $A_{kt}^{\text{new}}(u) = A_{kt}^{\text{new}}(R_{ti}(j))$. Remark that the atlas construction is largely similar to [2, 3].
Also, the atlas-to-image registration can be updated and we find following derivative:

$$\begin{aligned} \frac{\partial Q}{\partial R_{tij}} = 0 \Rightarrow \Bigg[\sum_k \rho_{itj} \frac{p_{itjk}}{\sum_{b(j)=1}^{8} w_{ib(j)t} A_{b(j)kt}} \sum_{b(j)=1}^{8} \\ \frac{\partial w_{ib(j)t}}{\partial R_{tij}} A_{b(j)kt} \Bigg] - \rho_{itj} \frac{(R_{tij} - G_{tj})}{\epsilon_{tj}^2} = 0 \end{aligned} \tag{5}$$

with $w_{ib(j)t}$ trilinear interpolation weights and $b(j)$ the neighbors of voxel j in the deformed atlas. It is clear that there is no closed

form solution, but the derivative gives direction to maximize the Q-function and hence to find an optimal deformation field. To obtain a physically acceptable deformation field, some form of regularization is required to impose local smoothness. This is performed by using the free-form registration approach of [7] where the derivative is interpreted as a force field to drive the viscous fluid regularizer by iteratively solving a simplified Navier-Stokes equation. Remark that the term ρ_{itj} can be seen as a weighting term to penalize the force field in voxels with a lower probability to belong to cluster t during the smoothing.
Finally, the prior on the clustering parameter can be updated:

$$\frac{\partial Q}{\partial \pi_{it}} = 0 \text{ s.t. } \sum_t \pi_{it} = 1 \Rightarrow \pi_{it} = \frac{1}{N_J} \sum_j \rho_{itj}. \qquad (6)$$

3. EXPERIMENTS AND RESULTS

Three different aspects of the algorithm can be validated: the clustering, the segmentation performance and the constructed probabilistic atlases. SPARC was implemented for the segmentation of the major brain tissue classes, i.e. white matter (WM), gray matter (GM) and cerebrospinal fluid (CSF), so validation will rely on these. Furthermore, in the algorithm, registrations are performed nonrigidly. Therefore, prior to performing SPARC, the images used in the experiments were affinely aligned with the MNI space using mutual information [15]. Our validation is based on two experiments.

3.1. Experiment 1

The first experiment makes use of twenty simulated MR images [16] and aims to validate the segmentation performance as a ground truth for white matter, gray matter and CSF is available. As all images are simulated from normal brain MR data, the number of clusters in the algorithm is fixed to one. The segmentation performance is measured in terms of the Dice overlap measure, i.e. Dice $= (2 \cdot |L_c \bigcap L_g|)/(|L_c| + |L_g|)$ with L_c the computed labels and L_g the ground truth.
The overlap measures and their standard deviation (std) are presented in Table 1. For comparison, also the Dice values of methods [9] and [14], called EEM and EMS, applied to the same data set, are presented. An example of a segmented image is also shown in Figure 2. It becomes clear that an accurate segmentation performance is obtained using our algorithm.

3.2. Experiment 2

The second experiment relies on two data sets. The first one contains eight MR images of healthy persons and the second one contains eight MR images of Huntington disease patients (HD). All images have image dimensions of $256 \times 256 \times 182$ and voxel sizes around 1mm^3. In this experiment, we validate the clustering, we take a look at the obtained probabilistic atlases and we compare the segmentation with the one obtained by using the EEM algorithm of [9]. Again, we use the Dice overlap measure and consider the segmentations obtained from EMS [14] as ground truth. The algorithm is initialized by setting the probabilities of all cluster parameters equal to a half. The initial estimations for the atlases equal the average over all images, giving one image that has a large probability to belong to that cluster a larger weight.

	WM	GM	CSF
SPARC	92.41 ± 0.85	90.47 ± 0.89	82.17 ± 2.90
EEM	89.67 ± 1.36	86.68 ± 1.84	70.76 ± 3.40
EMS	92.60 ± 0.74	90.63 ± 0.92	82.29 ± 3.00

Table 1. Dice coefficients and std $\times 100$ for Brainweb data.

	WM	GM	CSF
SPARC1	97.45 ± 0.39	93.24 ± 0.97	73.34 ± 6.12
EEM1	94.74 ± 0.90	88.66 ± 0.71	67.40 ± 5.51
SPARC2	97.36 ± 0.22	93.94 ± 0.46	82.76 ± 1.77
EEM2	93.38 ± 1.42	87.50 ± 1.27	76.45 ± 2.87

Table 2. Dice coefficients and std $\times 100$ for experiment 2 where the first two lines represent the results for the normal data (1) and the last two for the HD data (2).

We observe that 12 of the 16 images are classified in the correct cluster. For the four misclassified data, we remark that the cluster probabilities are much closer to a half. Furthermore, the wrong classified images are all HD images and less brain atrophy is present in these images than in the other HD images. Therefore, less deformation is necessary for registering those images to a normal image than to a HD with large brain atrophy. One can conclude that it would be more appropriate to include an extra cluster.
Morphological differences between both groups are made apparent in the constructed atlases and the clustering maps (Figure 3). For instance, a reduction in putamen and nucleus caudatus and an enlargement of the ventricles is clearly visible when comparing the atlas of the normal group against the atlas of the HD group. The clustering map represents the probability that a certain voxel belongs to a certain cluster. In Figure 3, we show the clustering map of a normal image to belong to the HD group. The blacker the voxel, the lower the probability to belong to that cluster. Remark, that the image intensities of this Figure are rescaled for visibility purposes, so white does not correspond with a probability of one to belong to that cluster. The morphological differences are again clearly visible.
The atlases are a good representation of the images belonging to the same cluster. Remark that the ventricles in the atlas of the cluster containing 'normal' data are slightly larger than those of an atlas constructed completely from brains of healthy persons, as the cluster also contains brain images of HD patients with small brain atrophy. The atlases are already quite sharp, but could have been sharper when allowing more deformation, in other words for a larger choice of the variance parameter ϵ^2.
Lastly, the segmentation performances of our algorithm for both the normal data (1) and the Huntington disease patients (2) are presented in Table 2 and two images are shown in Figure 2.

4. DISCUSSION AND CONCLUSION

In this paper we have presented a method for automatic segmentation and clustering of a set of brain MR images, which are both important aspects in the study of many neurological diseases for characterizing structural and functional differences and similarities between different (sub-)populations and for the localization of these differences. Also, our framework delivers completely automati-

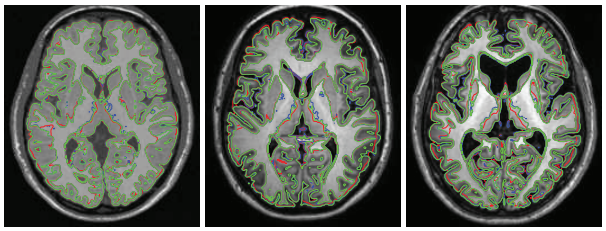

Fig. 2. Ground truth (blue) and segmentations obtained using SPARC (green) and EEM (red) of Brainweb data, normal data and HD data.

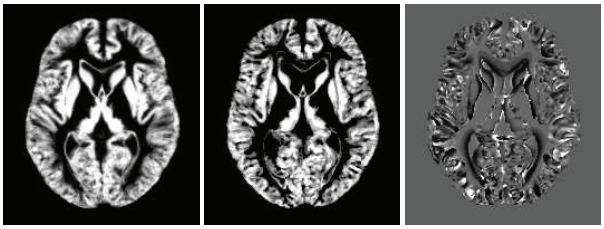

Fig. 3. From left to right: atlas for normal data, atlas for HD and clustering map for a normal image to belong to the HD cluster. Morphological differences are clearly visible, e.g. brain atrophy in putamen and nucleus caudatus and enlarged ventricles.

cally population-specific atlases which can later on serve as more appropriate prior information for more low-level segmentation approaches. Furthermore, the presented method is a mathematically comprehensive framework for a large part of recently published methods and where the different methods benefit from each other. Validation studies using restricted data sets show us promising results. Accurate segmentation results are obtained and different modes in a population can be traced. However, different parts of the algorithm can still be improved. The choice of the variance on the deformation field, determining the flexibility of the deformations, for instance is here chosen to be equal in each voxel and each direction. Instead, this parameter could be learned from a training data set and vary along different tissue classes, directions and for different diseases. Also, the prior on the clustering can be refined, for instance by giving a larger weight to regions where we expect to see differences. Therefore, future work will focus on improving the priors and on application driven studies.

5. REFERENCES

[1] B. Avants and J.C. Gee, "Geodesic estimation for large deformation anatomical shape averaging and interpolation," *NeuroImage*, vol. 23, pp. 139–150, 2004.

[2] S. Joshi, B. Davis, M. Jomier, and G. Gerig, "Unbiased diffeomorphic atlas construction for computational anatomy," *NeuroImage*, vol. 23(1), pp. 151–160, 2004.

[3] P. Lorenzen, M. Prastawa, B. Davis, G. Gerig, E. Bullitt, and S. Joshi, "Multi-modal image set registration and atlas formation," *MedIA*, vol. 10(3), pp. 440–451, 2006.

[4] K. Van Leemput, "Encoding probabilistic brain atlases using bayesian inference," *IEEE, Trans. Med. Img.*, vol. 28(6), pp. 822–837, 2009.

[5] M.R. Sabuncu, S.K. Balci, M.E. Shenton, and P. Golland, "Image-driven population analysis through mixture modeling," *IEEE Trans. Med. Img.*, vol. 28, pp. 1473–1487, 2009.

[6] M. Murgasova, D. Rueckert, D. Edwards, and J. Hajnal, "Robust segmentation of brain structures in MRI," *ISBI*, pp. 17–20, 2009.

[7] E. D'Agostino, F. Maes, D. Vandermeulen, and P. Suetens, "A viscous fluid model for multimodal non-rigid image registration using mutual information," *MedIA*, vol. 7(4), pp. 565–575, 2003.

[8] J. Ashburner and K.J. Friston, "Unified segmentation," *NeuroImage*, vol. 26, pp. 839–851, 2005.

[9] E. D'Agostino, F. Maes, D. Vandermeulen, and P. Suetens, "A unified framework for atlas based brain image segmentation and registration," *WBIR, LNCS*, vol. 4057, pp. 136–143, 2006.

[10] K.M. Pohl, J. Fisher, W.E.L. Grimson, R. Kikinis, and W.M. Wells, "A Bayesian model for joint segmentation and registration," *NeuroImage*, vol. 31, pp. 228–239, 2006.

[11] V. S. Petrovic, T. F. Cootes, C. J. Twining, and C. Taylor, "Automatic framework for medical image registration, segmentation and modeling," *MIUA*, vol. 2, pp. 141–145, 2006.

[12] K. K. Bhatia, P. Aljabar, J.P. Boardman, L. Srinivasan, M. Murgasova, S.J. Counsell, M.A. Rutherford, J. Hajnal, A.D. Edwards, and D. Rueckert, "Groupwise combined segmentation and registration for atlas construction," *MICCAI, LNCS*, vol. 4791, pp. 532–540, 2007.

[13] J. Xu, F. Liang, and L. Gu, "Bayesian co-segmentation of multiple MR images," in *ISBI*, 2009.

[14] K. Van Leemput, F. Maes, D. Vandermeulen, and P. Suetens, "Automated model-based bias field correction of MR images of the brain," *IEEE Trans. Med. Img.*, vol. 18(10), pp. 885–896, 1999.

[15] F. Maes, A. Collignon, D. Vandermeulen, G. Marchal, and P. Suetens, "Multimodality image registration by maximization of mutual information," *IEEE Trans. Med. Img.*, vol. 16(2), pp. 187–198, 1997.

[16] B. Aubert-Broche, M. Griffin, G.B. Pike, A.C. Evans, and D.L. Collins, "Twenty new digital brain phantoms for creation of validation image data bases," *IEEE Trans. Med. Img.*, vol. 25(11), pp. 1410–1416, 2006. *http://www.bic.mni.mcgill.ca/brainweb/*.